Molecular Therapy
Oncolytics
Original Article

# Enhancement of PSMA-Directed CAR Adoptive Immunotherapy by PD-1/PD-L1 Blockade

Inna Serganova,[1,4,5] Ekaterina Moroz,[1,4,5] Ivan Cohen,[2,5] Maxim Moroz,[3,4] Mayuresh Mane,[1,4] Juan Zurita,[3,4] Larissa Shenker,[3,4] Vladimir Ponomarev,[3,4] and Ronald Blasberg[1,3,4]

[1]Department of Neurology, Memorial Sloan Kettering Cancer Center, New York, NY 10065, USA; [2]Gerstner Sloan Kettering Graduate School of Biomedical Sciences, New York, NY 10065, USA; [3]Department of Radiology, Memorial Sloan Kettering Cancer Center, New York, NY 10065, USA; [4]Molecular Pharmacology and Chemistry Program, Memorial Sloan Kettering Cancer Center, New York, NY 10065, USA

**Chimeric antigen receptor (CAR) T cell therapy in hematologic malignancies has shown remarkable responses, but the same level of success has not been observed in solid tumors. A new prostate cancer model (Myc-CaP:PSMA(+)) and a second-generation anti-hPSMA human CAR T cells expressing a Click Beetle Red luciferase reporter) were used to study hPSMA targeting and assess CAR T cell trafficking and persistence by bioluminescence imaging (BLI). We investigated the antitumor efficacy of human CAR T cells targeting human prostate-specific membrane antigen (hPSMA), in the presence and absence of the target antigen; first alone and then combined with a monoclonal antibody targeting the human programmed death receptor 1 (anti-hPD1 mAb). PDL-1 expression was detected in Myc-CaP murine prostate tumors growing in immune competent FVB/N and immune-deficient SCID mice. Endogenous $CD3^+$ T cells were restricted from the centers of Myc-CaP tumor nodules growing in FVB/N mice. Following anti-programmed cell death protein 1 (PD-1) treatment, the restriction of $CD3^+$ T cells was reversed, and a tumor-treatment response was observed. Adoptive hPSMA-CAR T cell immunotherapy was enhanced when combined with PD-1 blockade, but the treatment response was of comparatively short duration, suggesting other immune modulation mechanisms exist and restrict CAR T cell targeting, function, and persistence in hPSMA expressing Myc-CaP tumors. Interestingly, an "inverse pattern" of CAR T cell BLI intensity was observed in control and test tumors, which suggests CAR T cells undergo changes leading to a loss of signal and/or number following hPSMA-specific activation. The lower BLI signal intensity in the hPSMA test tumors (compared with controls) is due in part to a decrease in T cell mitochondrial function following T cell activation, which may limit the intensity of the ATP-dependent Luciferin-luciferase bioluminescence signal.**

## INTRODUCTION

Prostate cancer is the second leading cause of cancer-related deaths in American men.[1,2] Although hormonal and radiation therapy can be very effective for local disease, patients usually become refractory to hormonal therapy (castration resistant) within 1–3 years. This is usually associated with the transition to a more aggressive form of the disease, leading to the development of bone and organ metastases. The addition of combination chemotherapy in the late stages of the disease has limited benefit, increasing survival for only several months.[3] Since most conventional treatments eventually fail, additional therapeutic strategies have been developed.[4] These therapeutic strategies have employed oncolytic viruses,[5] vaccines,[6] adjuvant immune modulation therapies (checkpoint inhibitors) (Slovin et al., 2012, J. Clin. Oncol, abstract), and adoptive immune cell (T cell) therapies.[7]

During the past 15 years, genetic engineering has been applied to more effectively direct T cells to tumor-expressing antigens, through the expression of specific chimeric antigen receptors (CARs) on an individual patient's T cells.[8–10] CARs consist of a tumor antigen-binding domain that is fused to an intracellular signaling domains and costimulatory receptors capable of activating T cells.[10–12] Therefore, antigen-recognition is not MHC-restricted, as is the case for T cell receptor (TCR)-mediated antigen recognition. In vivo efficacy of CAR-modified effector human and murine T cells has been demonstrated,[13–22] and prostate-specific membrane antigen (PSMA) is a promising molecular marker for targeted therapy of prostate cancer. PSMA is a glycosylated type-II membrane protein that is upregulated during malignant transformation in more aggressive prostate cancer, resulting in abnormally high levels of it on the cell surface.[23] We[24,25] and others[21,26–28] (Slovin et al., 2012, J. Clin. Oncol, abstract) have participated in developing imaging approaches to visualize anti-hPSMA CAR T cells and optimization of the structure of CARs to achieve more profound effects in the targeting of tumors bearing the corresponding antigen (hPSMA).

CAR T cell therapy in solid tumors has not achieved the clinical success that has been observed in hematologic malignancies.[29–31] One

Received 21 June 2016; accepted 29 November 2016;
http://dx.doi.org/10.1016/j.omto.2016.11.005.

[5]These authors contributed equally to this work.

**Correspondence:** Inna Serganova, Memorial Sloan Kettering Cancer Center, 1275 York Avenue, New York, NY 10065, USA.
**E-mail:** serganoi@mskcc.org
**Correspondence:** Ronald Blasberg, Memorial Sloan Kettering Cancer Center, 1275 York Avenue, New York, NY 10065, USA.
**E-mail:** blasberg@neuro1.mskcc.org

A

| Tumor | Doubling Time (days) | PSMA | Necrosis (H&E) | Blood Vessels (CD31) |
|---|---|---|---|---|
| Myc-CaP | 2.6 ± 0.6 | - | + | +++ |
| Myc-CaP:hPSMA | 2.7 ± 0.2 | +++ | + | +++ |

B

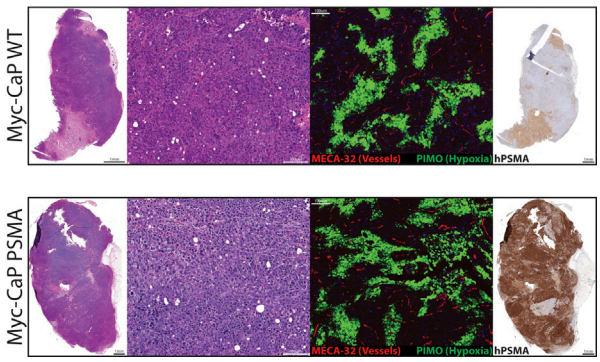


**Figure 1. Comparison of Myc-CaP Wild-Type and Myc-CaP:hPSMA(+) Tumors Growing in NOD.SCID Il2rg$^{-/-}$ (NSG) Mice**

(A) Mice received a s.c. injection of 1.0 × $10^6$ tumor cells; tumor growth was monitored and doubling time was calculated. H&E and immunofluorescence staining with MECA 32 (blood vessels are red) and Pimonidazole (hypoxia is green); scale bar, 100 μm. (B) Human PSMA was detected with PSMA (3E6 antibody, (Dako, Agilent Technologies).

reason for the poor treatment response is the failure of CAR T cells to accumulate and expand in the hostile tumor microenvironment.[32,33] The failure of a substantial CAR-mediated T cell response in solid tumors relates to a number of factors—including CAR T cell inactivation and possible exclusion from the tumor mass, the reciprocal interactions between tumor and stromal cells,[34–36] and propensity of cancer like prostate to disseminate preferentially to bone. Thus, preclinical studies that incorporate imaging to monitor T cell trafficking and activation are necessary to adequately explore the biology and efficacy of different treatment strategies designed to enhance T cell targeting and penetration of solid tumors. Several strategies have been employed to optimize the migration, survival, and effector functions of adoptive cell therapy (ACT) using TILs (tumor-infiltrated lymphocytes). For example, (1) increasing CXCR2 expression resulted in the improvement of T cell migration to tumors,[37] (2) genetic manipulation of IL-12 production by transferred T cells extends T cell survival,[38] and (3) the generation of novel CAR-based engineered T cells to improve tumor recognition and T cell activation[39,40] as well as the delivery of CAR T cells through specific polymer implants[41] or local injection.[22] Recently, it was demonstrated that CAR T cell therapy and programmed cell death protein 1 (PD-1) checkpoint blockade are a rational combination in a solid tumor model.[40]

Programmed death-ligand 1 (PD-L1)/PD-1-mediated T cell inhibition is involved in immune evasion in prostate cancer. Although only 1% PD-L1 cells were detected in prostate tumor samples,[42,43] immune cells (PD-1- and PD-L1-positive) were observed to surround prostate tumor nodules.[44] More recently, a novel monoclonal rabbit antibody to PD-L1 revealed that 62% human prostate tumors stain positive for PD-L1 expression.[45] The possibility that PD-L1/PD1-mediated T cell inhibition might be involved in immune evasion in prostate cancer is being explored in several clinical trials. Patients with metastatic castration-resistant prostate cancer (mCRPC) are being treated with anti-PD-1 antibody in two phase II clinical trials, involving pembrolizumab (Keytruda) and CT-011 (anti-PD-1 antibody; CureTech).[46,47]

The goal of this study was to study the efficacy of human hPSMA CAR-directed T cell therapy in an appropriate animal model. We show that anti-hPSMA CAR-directed T cell therapy of Myc-CaP:PSMA(+) tumors alone was unsuccessful, whereas the combination of anti-hPSMA CAR-directed T cells plus anti-hPD1 mAb immune modulation therapy provided a partial, short-duration and sub-optimal response.

## RESULTS

### Characterization of a New Murine Tumor Model for hPSMA-Directed CAR T Cell Therapy

Several prostate tumor models, both human and murine origins, have been described and used to study the targeting of hPSMA-CAR T cells, but some limitations have been identified.[21,24,48,49] We focused on murine cell lines, with prospective to utilize them in a syngeneic mouse model using immunocompetent mice. We chose a well established and studied murine prostate cancer cell line, Myc-CaP,[50] for our initial studies. Myc-CaP tumors are composed of sheets and indistinct lobules/nests of polygonal to oval cells separated by fine fibrovascular straie, as described previously.[50] Tumor cells have abundant amphophilic cytoplasm and large, round to polygonal nuclei. Necrosis is rare in small tumors; larger tumors have more extensive necrosis. The percentage of necrosis varied from 2% to 25%, depending on the overall tumor mass (Figure 1).

To generate an appropriate murine model for the anti-hPSMA CAR T cell therapy, wild-type (WT) Myc-CaP cancer cells were stably transduced with a hPSMA-containing retroviral vector and sorted as described in Materials and Methods (Figure S1A).[24,51,52] We compared the growth profiles of wild-type and hPSMA(+) Myc-CaP tumors in mice, and found no significant difference in tumor doubling time, morphology, extent of necrosis (Figure 1A), or level of tumor hypoxia (Figure 1B). The only difference was that Myc-CaP:hPSMA(+) tumors stained strongly positive for hPSMA, whereas WT Myc-CaP:hPSMA(−) tumors did not (Figure 1B).

### Second-Generation Anti-hPSMA CAR Cytotoxic T Lymphocytes Targeting Myc-CaP:hPSMA(+) Tumors

T cells derived from human blood were isolated,[24] activated, and transduced with a newly developed retroviral second-generation

anti-hPSMA CAR Plg28z vector and with SFG-tdRFP/CBRLuc vector. Reproducible levels of hPSMA CAR expression on transduced human T cells were observed (Figure S1B).[24,53] Cytotoxicity studies revealed that hPSMA targeted CAR T cells have a 13.8 + 5.9% cytolytic efficacy against Myc-CaP:hPSMA(+) cells, when the ratio of the effector to the target is 40 to 1. However, the same hPSMA-targeted CAR T cells showed 2-fold higher cytotoxic activity toward a human prostate cancer cell line PC3/PSMA-IRES-Puromycin (PC3-PIP) (Figure S1C).

### Bioluminescence Imaging of Anti-hPSMA CAR T Cell Targeting Myc-CaP:hPSMA(+) Tumors

Using two distinct luciferase reporter systems, we were able to image the location of Myc-CaP tumors with the Renilla luciferase (Rluc) reporter[54] and image the trafficking of anti-hPSMA CAR T cells with the tdRFP/CBRLuc reporter. First, we assessed the capacity of systemically administered anti-hPSMA CAR T cells to traffic and accumulate within established subcutaneous Myc-CaP:hPSMA(+) tumors. When tumors reached ~50–100 $mm^3$ size, mice were injected intravenously with $20 \times 10^6$ anti-hPSMA CAR T cells (~87% of T cells had anti-hPSMA CAR expression, and ~67% of CAR-positive T cells were also positive for the tdRFP/CBRLuc fusion reporter). Bioluminescence imaging (BLI) following i.v. injection of anti-hPSMA CAR T cells was performed on 0, 1, 5, 9, and 12 days after administration. Initially, CAR T cells sequestered in the lungs for up to 9–10 days, as visualized by BLI (Figure S2A). Their presence in lungs was confirmed by $CD3^+$ immunohistochemistry (IHC) staining (Figure S2B). A minimal BLI signal was observed within Myc-CaP:hPSMA(+) tumors during the first 48 hr, suggesting that some CAR T cells trafficked to the tumor. However, only a minimal (non-statistically-significant) response of anti-hPSMA CAR T cell therapy was observed on tumor growth/volume, compared with control (no CAR-T cells treated) tumors (Figure S2C).

To further evaluate in vivo therapeutic efficacy of anti-hPSMA CAR-transduced T cells, we performed "pre-targeting" experiments using the Winn assay (Figure 2).[55] Anti-hPSMA CAR T cells alone or mixed with Myc-CaP:hPSMA(+) or Myc-CaP:hPSMA(−) target cells were prepared just prior to subcutaneous inoculation into NOD.SCID Il2rg−/− (NSG) mice; the inoculum included a 1:10 tumor-to-T cell ratio, mixed in growth media and Matrigel Matrix (1:1) at 4°C. The location of the tumor was identified using Renilla Luciferase BLI (Figure 2A). We also monitored tumor growth by BLI (Figure 2C) (in addition to caliper measurements; Figure 2D) until the point where the tumors reached a size where the BLI Renilla Luciferase signal was saturated and tumors showed evidence of necrosis (day 15; Figure 2C).

Progressive tumor growth was observed in the two "control groups" of mice: (1) mice injected with Myc-CaP:hPSMA(+) tumors alone (without CAR T cells) and (2) Myc-CaP:hPSMA(−) tumors (without hPSMA expression) but mixed with anti-hPSMA CAR T cells (Figures 2A, 2C, 2D). A marked reduction in tumor growth rate was observed in the "test group" of mice: tumors that developed from the mixture of Myc-CaP:hPSMA(+) cells and anti-hPSMA CAR T cells (Figures 2A, 2C, 2D). By day 26, the "test group" tumor size was 224 ± 240 $mm^3$, whereas the size of control tumors without anti-hPSMA CAR T cell inclusion was significantly larger, 1,676 ± 406 $mm^3$ ($p < 0.05$). The "pre-targeting" (Winn assay) experiments clearly demonstrate that anti-hPSMA CAR T cells can inhibit Myc-CaP:hPSMA(+) tumor growth and that this inhibition is hPSMA dependent.

The persistence of anti-hPSMA-targeted CAR T cells in the same Winn assay described above; T cells were monitored by the CBRLuc/luciferin BLI signal generated from the reporter-transduced CAR T cells (Figures 2B and 2E). We observed that anti-hPSMA CAR T cells injected alone in Matrigel matrix (control, in the absence of any tumor cells) were localized at the site of injection and were visualized over 8 days. However, the presence Myc-CaP tumor cells (with or without human PSMA/antigen) notably influenced the BLI signal intensity at the injection site. Since the intensity of the BLI signal has been used as indicator of the injected CAR T cells, the difference in BLI signal suggested that the survival of CAR T cells was different in the three study groups. The BLI signal from CAR T cells was visualized longest (~8 days) when they were injected alone (non-tumor group), less in the hPSMA(−) tumor group (~6 days), and least in the hPSMA(+) tumor group (~4 days). These data suggest that BLI detection and the survival of CAR T cells was shortened by the presence of hPSMA(+) on tumor cells. Interestingly, this group demonstrated a better treatment response (Figure 2D).

### Metabolism of hPSMA CAR T Cells

It is known that T cells undergo a transition from a quiescent to a highly active effector phenotype upon stimulation/activation and transduction with the anti-hPSMA CAR vector. This transition also involves a significant shift from oxidative to glycolytic metabolism. To study the metabolic status of T cells during activation, transduction, and proliferation, we measured the extracellular acidification rate (ECAR) and the oxygen consumption rate (OCR) of these cells. The rate of glycolysis (ECAR), as well as basal and maximal OCRs (an indicator of mitochondrial respiration), was assessed on days 2, 8, 10, and 15 of CAR T cell preparation (Figure 3). Human T cells from three donors were isolated from buffy coat using Ficoll separation. Forty-eight hours after phytohemagglutinin (PHA) stimulation, cells were transduced with a retroviral vector bearing a CAR targeting hPSMA. We obtained a measure of ECAR in naive T cells, T cells stimulated by PHA and hPSMA CAR-transduced T cells (Figure 3A). Naive non-stimulated T cells demonstrated low levels of glycolysis, whereas non-specific PHA stimulation of T cells results in a significant ($p < 0.05$) increase in glycolysis, that is maintained at high levels over the course of T cell transduction and expansion (Figure 3A). The initial increase in a basal mitochondrial respiration after non-specific PHA stimulation is followed by a progressive decline in mitochondrial function during subsequent procedures (Figure 3B). FCCP (carbonyl cyanide *p*-trifluoromethoxy phenylhydrazone) was added to uncouple oxidative phosphorylation from the electron transport chain to measure the maximum respiratory capacity.[56]

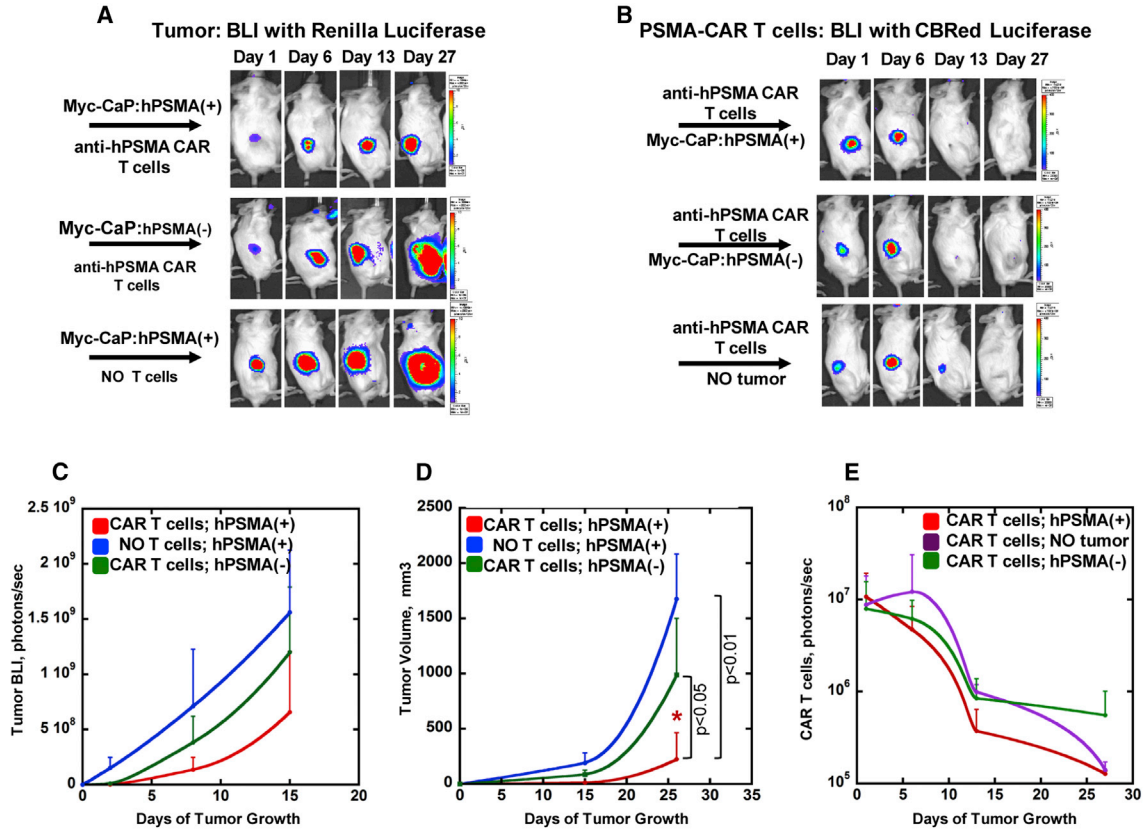


**Figure 2. Pre-targeting of Anti-hPSMA CAR-Directed Human T Cells to Myc-CaP:hPSMA(+) and Myc-CaP:hPSMA(–) Tumor Cells: Winn Assay**

(A) BLI images of tumor burden in different experimental sets: PSMA-directed CAR T cells mixed with (i) Myc-CaP:hPSMA(+) or (ii) Myc-CaP:hPSMA(–) tumor cells (the Winn assay), and (iii) a control set (Myc-CaP:hPSMA(+) tumor cells alone, no CAR T cells). (B)BLI images of anti-hPSMA CAR T cell in different treatment sets: PSMA-directed CAR T cells mixed with (i) Myc-CaP:hPSMA(+) or (ii) Myc-CaP:hPSMA(–) tumor cells (the Winn assay) and (iii) a control set (PSMA-directed CAR T cells alone, no tumor cells). Tumor growth profiles in NOD.SCID Il2rg–/– (NSG) mice following different treatment regimens. (C) Tumor growth was monitored by BLI using a Renilla Luciferase/coelenterazine reporter in tumor cells through day 15. (D) Tumor growth was monitored by caliper measurements. PSMA-directed CAR T cells significantly delayed the growth of hPSMA(+) tumors, compared with hPSMA(–) tumors and non-treated hPSMA(+) tumors; tumor volume measurements were significantly different on days 15 and 27. (E) Time-course of the BLI signal from anti-hPSMA CAR T cells in different experimental groups; BLI signal intensity from anti-hPSMA CAR T cells was lower in the hPSMA(+) tumors compared to hPSMA(–) tumors on days 12 and 27, and significantly lower than CAR T cells injected alone (in the absence of tumor cells) on days 7 and 12 but not on day 27. The number of mice per group, n = 5.

The maximum respiratory rate (OCR) was significantly higher at day 2 after PHA stimulation but declined by day 8 (Figure 3C). Similar results were obtained for CAR-transduced T cells, showing low mitochondrial function following anti-hPSMA CAR transduction (Figures 3B and 3C).

### Limited Dissemination of Endogenous T Cells in PD-L1-Positive Myc-CaP Tumors

To assess the associations between PD-L1/PD-1 signaling and T cell targeting of Myc-CaP tumors, and the impact on tumor progression, we performed immunofluorescence staining for PD-L1 in (1) Myc-CaP:hPSMA(+) tumors growing in NOD.SCID mice and (2) Myc-CaP WT tumors growing in immune-competent FVB/N. Both tumors stained positive for PD-L1 (Figure 4A). The spatial distribution of $CD3^+$ T cells in Myc-CaP WT tumors (growing in FVB/N mice) was also examined; a predominance of T cells was observed along the invasive tumor margin (stromal-tumor edge), with reduced numbers in the center of the tumor (Figures 4B and 5C, upper panel). We then evaluated whether anti-murine programmed death-ligand 1 (mPD-1) mAb treatment increased the number of tumor-infiltrating lymphocytes in subcutaneous Myc-CaP tumors (FVB/N mice). We administrated 5 doses of 200 μg of anti-mPD1 mAb per mouse (on days 9, 11, 13, 15, and 17 after tumor cell injection) and observed a significant delay ($p < 0.05$) in tumor growth (Figure 5A), which continued even after mice stopped receiving anti-mPD1 therapy. Interestingly, tumors <50 $mm^3$ responded to the anti-mPD1 mAb treatment, whereas larger tumors failed to respond to the treatment (Figure 5A).

The density of $CD3^+$ T cells per square millimeter of tumor area (Figures 5B and 5D), T cell size (Figure 5D) and the correlation between these two parameters and T cells distribution along the tumor edge

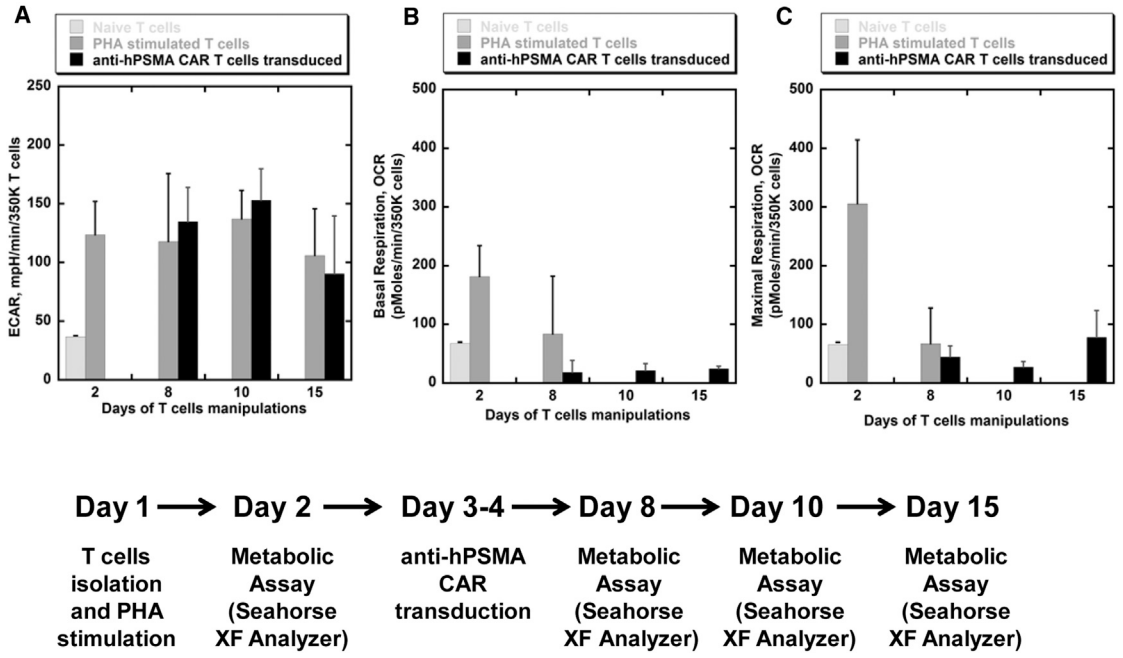


**Figure 3. Effect of T Cell Processing on Their Metabolic Properties**

(A and B) Changes in ECAR (A) and OCR (B) following the processing of T cells from a post harvesting, "naive" status to anti-hPSMA CAR reporter bearing T cells. To assess glycolytic function, T cells were initially incubated in medium without glucose and ECAR is assessed. The first injection is a saturating concentration of glucose (25 mM), where glucose is taken up by the cells and catabolized through the glycolytic pathway to lactate, producing ATP and protons. (A) The extrusion of protons into the surrounding medium produces a rapid increase in ECAR. This glucose-induced response is reported as the rate of glycolysis (or glycolytic flux) percent increase over basal conditions. (B and C) In the mitochondrial respiration assay, basal OCR (B) is measured under full media growing conditions, followed by sequential addition of oligomycin, FCCP (C), maximal respiration) and antimycin A/rotenone with a measurement of changes in OCR. Each data point represents mean ± SD, n = 8. Data are normalized to 350,000 cells.

was evaluated (Figure 5C). A marked increase (~13-fold) in $CD3^+$ T cell density was observed in central tumor areas following anti-mPD1 therapy (Figure 5D). We also noticed that T cell size increased in responder tumors from 40 ± 15 $\mu m^2$ (IgG treated) to 51 ± 23 $\mu m^2$ (anti-mPD1 treated) but not in the non-responding tumor (42 ± 15 $\mu m^2$). A comparison of $CD3^+$ T cell distribution over the tumor sections showed that $CD3^+$ T cells predominantly localized along the rim of tumor nodules prior to and following anti-PD1 treatment, even though the restriction of $CD3^+$ T cells from the center of the tumor nodules was reversed (Figure 5C). No significant difference was observed in CD31 blood vessel staining of the tumors (data not shown).

### Anti-hPD1 mAb Treatment Enhances Adoptive Anti-hPSMA CAR-Mediated T Cell Therapy

Encouraged by the response of Myc-CaP WT tumors to anti-mPD1 mAb treatment in FVB/N mice, we evaluated the effect of anti-hPD1 treatment combined with anti-hPSMA CAR T cell adoptive therapy in the Myc-CaP:hPSMA(+) and Myc-CaP:hPSMA(−) tumor models. Anti-hPSMA CAR T cells (transduced with the CBRluc reporter) were monitored by BLI at different time points after i.v. administration (days 0, 1, and 6) (Figure 6B). Ten minutes following CAR T cell injection, the T cells were localized largely in the lungs of all animals, with a variable low intensity signal appearing in the area of the tumors (Figure 6B). Interestingly, the highest tumor-associated T cell BLI signal was observed in the Myc-CaP: hPSMA(−) tumors (anti-hPD1-treated control group), and the lowest signal was observed in the Myc-CaP:hPSMA(+) tumors (anti-hPD1-treated test group). Nevertheless, Myc-CaP:hPSMA(+) tumor-bearing mice receiving the combined treatment (both anti-hPSMA CAR T cells ($10 \times 10^6$) and anti-hPD-1 mAb; test group) had a significant ($p = 0.03$, $p = 0.04$) treatment response (tumor volume), when compared to the two control groups (Figures 6C and 6D). The absence of a treatment response in Myc-CaP:PSMA(−) tumors (anti-hPD1 mAb-treated control group), despite the more robust T cell trafficking-to and BLI signal-in the tumor region is of particular interest.

A comparison of CAR T cell BLI signals from tumors and lungs during the first 24 hr showed that the BLI signal in the tumors was more stable (Figure S3A) compared with that in the lungs (Figure S3B), where a decline in signal intensity was observed in all treatment groups. By day 6 after anti-hPSMA CAR T cell injection, there was near total fading of the BLI signal from the lungs, whereas a longer-lasting BLI signal in the tumor areas was observed (Figure 6B). Following the cessation of anti-hPD1 treatment (day 20), we observed an increase in tumor growth of hPSMA(+) positive tumors treated with both anti-hPD1 mAb (five doses) and anti-hPSMA CAR T cells (one dose injection), comparable with other groups of mice (Figure 6C).

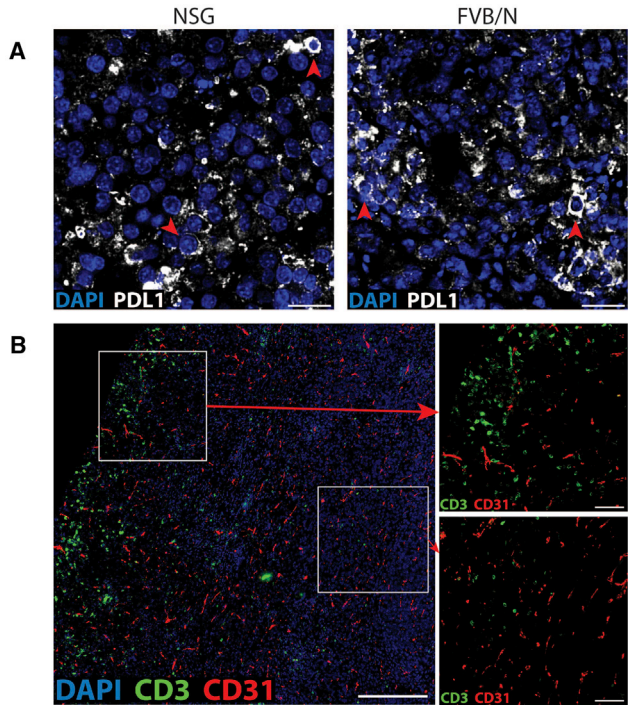


**Figure 4. Limited Distribution of Endogenous T Cells in PD-L1-Positive Myc-CaP Tumors**

(A) PD-L1 expression in Myc-CaP:hPSMA(+) tumors growing in NOD.SCID Il2rg$^{-/-}$ (NSG) mice on day 27 and MyC-CaP:WT in FVB/N mice on day 20 was studied by immunofluorescence imaging (IF). (B) CD3$^{+}$ T cells are excluded from the core of Myc-CaP:WT tumor cell nests, and are present at high density in the tumor periphery; scale bar, 200 μm for the large image and 50 μm for the insets.

H&E staining of one tumor from each treatment group shows different levels of necrosis 24 hr after initiation of treatment (Figure 7). hPSMA(+) tumors treated with both anti-hPD1 mAb and anti-hPSMA CAR T cells (test) showed the most necrosis (Figure 7A), whereas both control tumors showed considerably less necrosis (Figures 7B and 7C). The density of TUNEL positive cells showed a similar pattern; 54 TUNEL (+) cells/mm$^2$ were detected for the test group (hPSMA(+), anti-hPD1), whereas 29 and 26 TUNEL$^{+}$ cells were observed in the anti-IgG, hPSMA(+) and anti-hPD1, PSMA(−) control groups, respectively (Figure 7, far right column). The distribution and density of anti-hPSMA CAR T cells was higher in the center of a hPSMA(+) tumor treated with anti-hPD1 mAb at day 6 compared to controls (Figures S4 and S5), although more CAR T cells were localized along the periphery of these tumors (Figure S4). In contrast, CD31 staining of the tumors following 6 days of combined treatment showed no difference in microvessel density (Figure S5).

## DISCUSSION

CAR T cell therapy for hematologic malignancies has shown some remarkable success in recent years.[29,30,39,57,58] We focused on hPSMA targeting in prostate tumors using human anti-hPSMA CAR T cells, because of an existing clinical trial at our institution (MSKCC) (clinical trial #NCT01140373, https://clinicaltrials.gov) (Slovin et al., 2013,J. Clin. Oncol., abstract). It has been shown that adoptive transfer of T cells modified with the anti-hPSMA CAR could specifically mediate regression of pulmonary experimental lung metastasis in SCID mice.[21,24,49] However, this approach was ineffective against established subcutaneous tumors,[49] unless the CAR T cells were injected locally.[49]

To evaluate the effectiveness of second-generation anti-hPSMA CAR T cells in a pre-clinical setting, we developed the Myc-Cap (hPSMA$^{+}$) tumor model in immune deficient mice (NOD.SCID Il2rg$^{-/-}$, NSG). The Myc-CaP murine prostate cancer model was chosen to investigate hPSMA-directed adoptive CAR T cell therapy for the following reasons: (1) Myc-CaP s.c. tumors are slow-growing (allowing time for immune targeted therapy) and can be used in a syngeneic mouse model using immune competent mice; (2) moderate size tumors have little necrosis (reducing confounding factors in the interpretation of results); (3) a genetically modified Myc-CaP cell line with high cell-membrane localized PSMA expression was developed to allow direct comparisons between PSMA(+) and PSMA(−) tumors; (4) both PSMA(+) and PSMA(−) tumors had very similar growth and morphological characteristics (Figure 1).

This study focuses on the potential for enhancing the efficacy of hPSMA CAR-directed T cell therapy using an immune checkpoint inhibitor (PD-1L/PD1 blockade) just prior to i.v. administration of CAR T cells. Our initial efforts to evaluate the effectiveness of second-generation anti-hPSMA CAR T cells[24,53] were comparable to that of others (Figure S2).[49] Namely, anti-hPSMA CAR T cell therapy alone was not effective against established subcutaneous Myc-Cap hPSMA(+) tumors. Nevertheless, a Winn assay[55] demonstrated that anti-hPSMA CAR T cells can inhibit Myc-CaP:hPSMA(+) tumor growth in a scarce nutrient microenvironment, and that this inhibition is hPSMA dependent. However, Myc-CaP:hPSMA(+) tumors re-grew in 3 weeks after implantation (Figures 2C and 2D).

The finding that Myc-CaP tumors are PD-L1 positive in both an immunocompromised and immunocompetent mice raised the question whether the restriction of CD3$^{+}$ T cells from the interior of Myc-CaP WT tumors in FVB/N mice was related to PD-L1/PD1 engagement (Figure 4B). A similar exclusion of CD3$^{+}$ T cells was described in metastatic melanoma[59] and other types of cancer.[60,61] Given that PD-1 receptor expression is increased on activated T cells following engagement with PD-L1 ligand and high PD-L1/PD1 expression is associated with T cell exhaustion,[59,62] we treated Myc-CaP WT tumors in FVB/N with anti-mPD1 mAb and observed a significant, but only a partial delay in tumor growth (Figure 5A). Although based on a small number of animals (n = 5), we observed a ~13-fold increase in intratumoral CD3$^{+}$ T cell density following anti-PD1 inhibition (Figure 5B), consistent with releasing the PD-1 immune checkpoint and leading to T cell proliferation, intratumoral infiltration and increased effector function.[63] We also observed that T cells changed their morphology and increased in size following

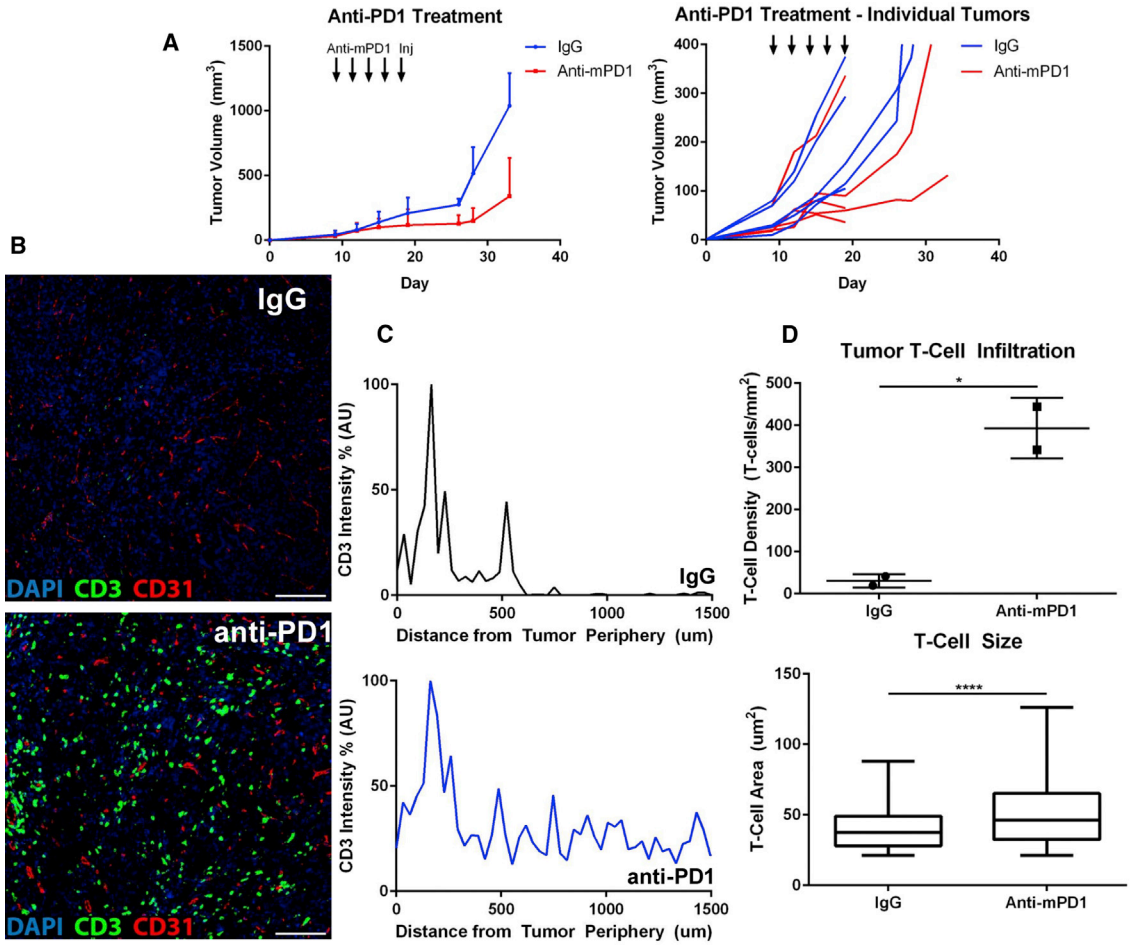


**Figure 5. The Effect of the PD-1/PD-L1 Axis Blockade on Myc-CaP WT Tumors**

(A) The effect of anti-mPD1 mAb treatment compared to non-specific IgG treatment (control) on the growth of wild-type Myc-CaP tumors in FVB/N mice; n = 5 animals per group. (B) Immunofluorescence imaging (IF) of $CD3^+$ T cells in the center of an IgG-treated (control) and an anti-mPD1 mAb-treated (test) tumor; scale bar, 100 μm. (C) Profile of $CD3^+$ T cells fluorescence (from tumor periphery to center) of IgG (control) and anti-mPD1 (test) treated animals. (D) Comparison of $CD3^+$ T cell density (number per square millimeter tumor area), and T cell size in control and test groups.

anti-mPD1 mAb treatment, consistent with cell cycle activation and proliferation.[64,65] Although this suggests that anti-mPD1 mAb treatment resulted in increased $CD3^+$ T cell activation, proliferation, and effector functions, the response was limited and indicates other factors are involved.

Nevertheless, the encouraging response of wild-type Myc-CaP tumors to anti-mPD1 mAb treatment in immune competent FVB/N mice led us to evaluate the effect of anti-hPD1 mAb treatment in combination with hPSMA-targeted CAR T cells in the Myc-CaP:hPSMA(+) tumor model. In these adoptive CAR T cell experiments, we first showed that combined treatment with anti-hPD1 antibody significantly inhibited Myc-CaP:hPSMA(+) tumor growth (Figure 6C) and that the antitumor response mediated by this combined therapy was both anti-hPD1 and hPSMA specific. Namely, the IgG-treated control group did not show an inhibitory effect, nor did tumors that were hPSMA(−). The blocking of hPD-1 enhanced the anti-tumor effect of hPSMA-targeted CAR T cells (Figure 6C), even in the presence of murine PD-L1 in the target tumors (Figure 4). The treatment response was confirmed by H&E and TUNEL staining of the tumor 24 hr after initiation of treatment (Figure 7A). These results suggest that there is a direct impact of PD-1 blockade on CAR T cell cytolytic function in these tumors.

Anti-PD1 mAb treatment of Myc-CaP WT tumors growing in immune-competent FVB/N mice had a more profound and prolonged effect, even following treatment withdrawal (Figure 5A). This effect was greater than a single injection of anti-hPSMA CAR T cells and five doses of anti-hPD1 mAb treatment of Myc-CaP:hPSMA(+) tumors growing in NSG mice (tumor growth was delayed for only 10 days). We suggest that anti-hPD1 antibody treatment combined with anti-hPSMA CAR human T cells had enhanced killing capacity

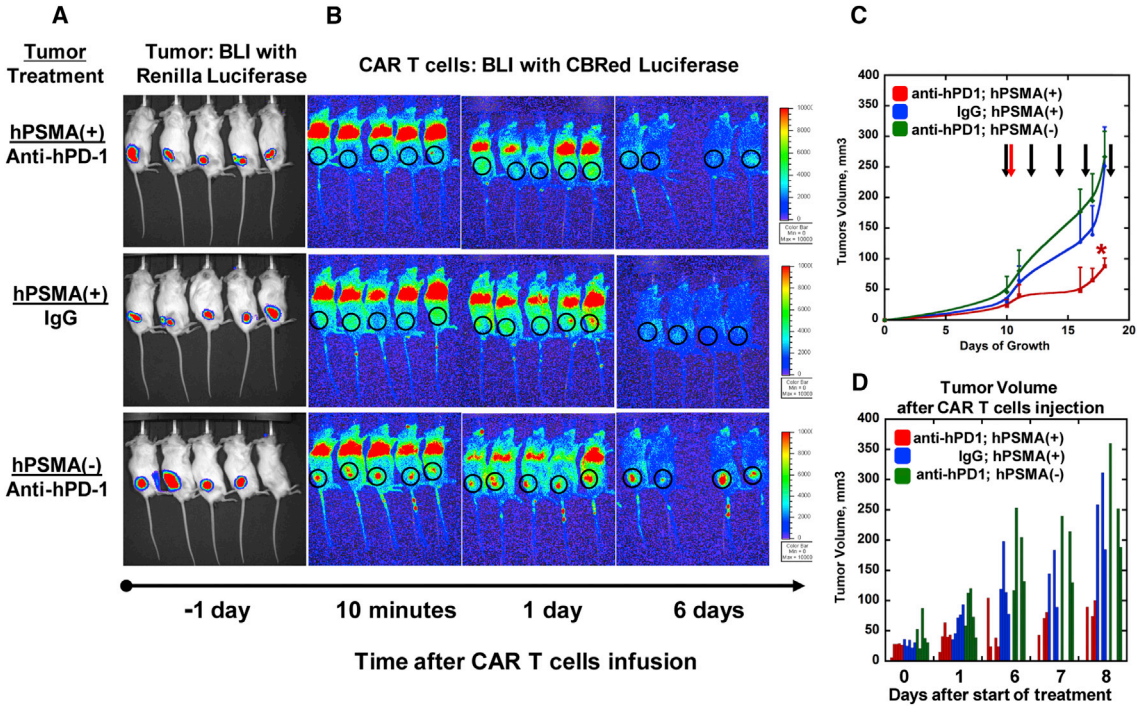


**Figure 6. Anti-hPD1 mAb Treatment Enhances Adoptive Anti-hPSMA CAR-Directed T Cell Therapy**

(A) Bioluminescence imaging of Myc-CaP:hPSMA(+) and Myc-CaP:hPSMA(−) tumors (transduced with the Rluc reporter) in NOD.SCID Il2rg$^{-/-}$ (NSG) mice to confirm tumor location. (B) Bioluminescence imaging of anti-hPSMA CAR T cells (transduced with the tdRFP/CBLuc reporter) 10 min after i.v. infusion and at 1 and 6 days. T cells trafficked largely to the lungs, although some localization to the tumor regions was visualized. (C) Plot of the mean tumor volume, comparing three treatment groups of mice (n = 5 per group). Treatments with anti-hPD1 mAb (test) or IgG mAb (control) are indicated by the black arrows; i.v. administration of anti-hPSMA CAR T cells is indicated by the red arrow. p value across groups is given for a one-tailed t test, *$p < 0.05$ versus control Myc-CaP:hPSMA(−) with anti-hPD1 mAb tumors and Myc-CaP:hPSMA(+) with IgG mAb. (D) A comparison of tumor growth in individual mice after the initiation of treatment; three groups are compared: anti-hPD1 mAb treatment of hPSMA(+) tumors (test), non-specific IgG treatment of hPSMA(+) tumors (control), and anti-hPD1 mAb treatment of hPSMA(−) tumors (control, no PSMA target).

and cytokine function against Myc-CaP:hPSMA(+) tumors, although the treatment response was comparatively short in duration. Recent literature[40,66] demonstrates that adoptive immunotherapy using genetically modified T cells in combination with PD-1 checkpoint blockade can enhance the antitumor effects of CAR T cells against established subcutaneous tumors in an immune compromised host. Nevertheless, our results indicate that other immune modulation mechanisms exist and restrict CAR T cell targeting, function, and persistence in hPSMA expressing Myc-CaP tumors.

Rapid destruction of i.v. administered CAR T cells is well known.[49,67] Nevertheless, the persistence of CAR T cells is well documented in the treatment of many "liquid" tumors,[68–70] whereas the persistence of CAR T cells is not a common finding in the treatment of solid tumors.[71] Previous studies have shown that the therapeutic efficacy of adoptive T cell transfer is correlated with the ability of T cells to proliferate and survive in vivo.[72] To address this issue, we used bioluminescence reporter-gene imaging (BLI) and immunofluorescence staining to track adoptively administered CAR T cells. In our BLI studies, there was a clear difference in anti-hPSMA CAR T cell trafficking to and initial persistence in Myc-CaP tumors (with and without the presence of the target antigen - hPSMA), even during the first minutes after T cells injection (Figures 6A and 6B). This difference in BLI signal was present over days 0, 1, and 6 following CAR T cells injection (Figure 6B). The seemingly contradictory T cell BLI and treatment response observations (Figures 2B, 2E, 6B, and 6C) and inconsistencies between T cell BLI (Figure 6) and CD3$^+$ staining for T lymphocytes (Figure S5), can be explained in several ways.

We performed our experiments thinking that CBRLuciferase (CBRluc) BLI could be used as a readout of CAR T cell number and persistence. To explain the above observations, we assumed the anti-hPSMA CAR T cells were undergoing more rapid destruction in hPSMA(+) Myc-CaP tumors compared to hPSMA(−) tumors, since the T cells were bearing a second generation CAR. To confirm this hypothesis, we detected more apoptotic CAR T cells in co-culture experiments with hPSMA(+), than with hPSMA(−) Myc-Cap tumor cells (data not shown). Anti-hPSMA CAR T cells in the absence of the hPSMA are likely to remain in a non-activated (anergic) state and not be subject to PSMA antigen-induced activation leading to T cell death/destruction.[73] Therefore, it was reasonable to consider that "quiescent T cells" could survive for a longer period of time and be visualized by BLI.

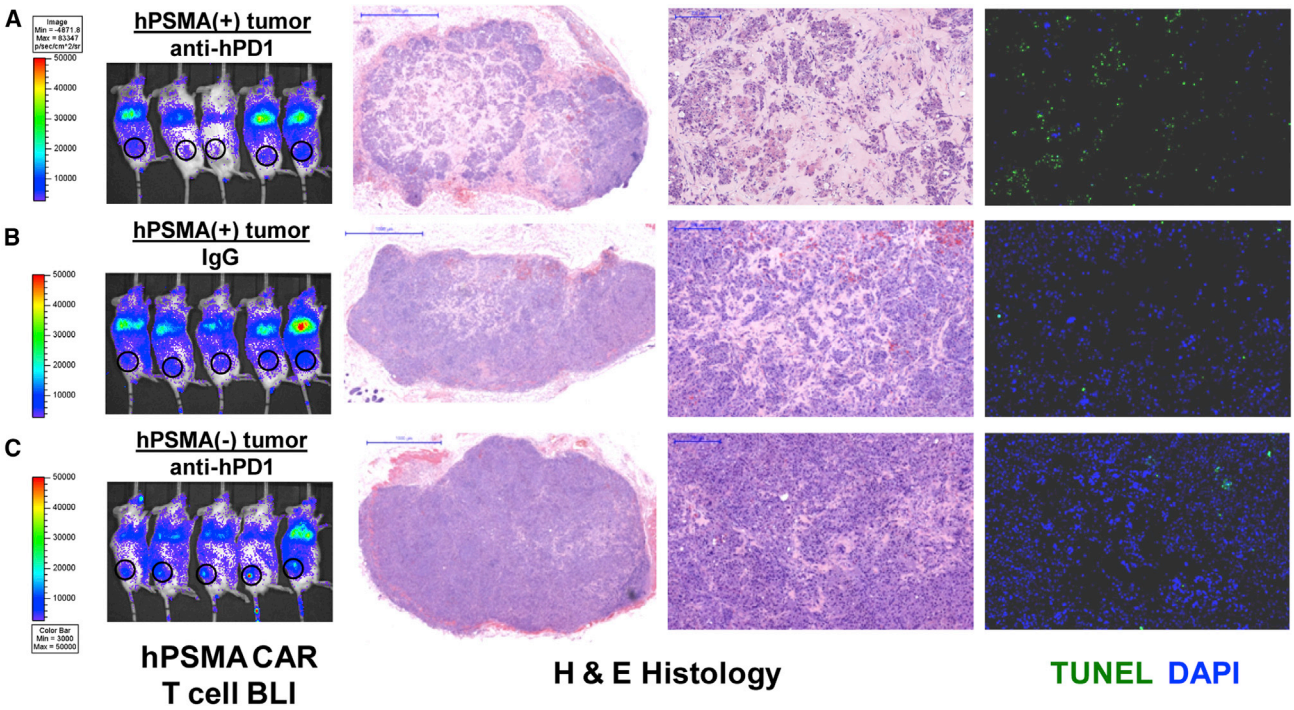


**Figure 7. Distribution of Anti-hPSMA CAR T Cells at 24 hr and Analyses of Tumor Treatment Response**

A comparison of three treatment groups: (A) anti-hPD1 mAb treatment of Myc-CaP:hPSMA(+) tumors (test), (B) non-specific IgG treatment of Myc-CaP:hPSMA(+) tumors (control), and (C) anti-hPD1 mAb treatment of Myc-CaP:hPSMA(−) tumors (control, no PSMA target) in combination with an i.v. infusion of $10 \times 10^6$ anti-hPSMA CAR T cells. Scale bars are 1 mm for the second column and 200 μm for the third and fourth columns. TUNEL(+) cells per square millimeter were 54 (A), 29 (B), and 26 (C), respectively.

An additional and more plausible explanation is that following contact with tumor cell membrane-localized hPSMA, the anti-hPSMA CAR T cells undergo a transition from a quiescent to a highly active effector phenotype. This transition also leads to a significant shift in the metabolism of hPSMA CAR T cells, from a TCA cycle and oxidative phosphorylation OXYPHOS-based metabolism,[74] to a more glycolysis-dependent metabolism to support macromolecule synthesis, proliferation, and effector function[75]). These changes in the metabolism of CAR T cells transitioning from a quiescent to an activated state could directly affect CBRluc BLI signal intensity. Recently, it was observed that activated tumor-infiltrating T cells display a phenotype of metabolic insufficiency, characterized by a persistent loss of mitochondrial function and mass.[76] Additionally, it was shown that chronic activation of T cells (associated with an anti-cancer response) represses oxidative metabolism, concomitant with a loss of mitochondrial mass and function, and that a significant decrease/loss of ATP was observed in activated $CD8^+$ T cells.

In light of these observations[76] and the data provided in Figure 3 showing lower mitochondrial activity in CAR T cells, we suggest that activated T cells can be associated with a low BLI readout (photons) using luciferin-luciferase-based reporter systems. The Click Beetle Red Luciferase (CBRluc) reporter is dependent on the presence of intra-cellular ATP, since this reporter belongs to the class of oxidative enzymes catalyzing the reaction of luciferin+ATP leading to formation of oxyluciferin, AMP and light. Therefore, the CBRluc reporter (and other ATP-dependent luciferases, including Firefly luciferase) is dependent on the presence of saturable amounts of ATP for reliable BLI measurements of reporter-cell number and persistence.[77] Interestingly, several other investigators have found that Firefly luciferase is not an optimal reporter for tracking activated T cells[78,79] (as well as unpublished conversations with other investigators).

There are several limitations to this study. First is the very short life of anti-hPSMA CAR T cells in the presence of hPSMA(+) Myc-CaP cells/tumors compared with hPSMA(−) cells/tumors, which leads to their longer persistence in the Winn assay (control group, hPSMA(−) tumors). Second is a modest cytotoxicity of CAR T cells (Figure S1) to murine cancer cells bearing hPSMA, which leads to Myc-CaP:hPSMA(+) tumor progression after 3 weeks in the Winn assay (Figures 2C and 2D) compared with total eradication of PC3/PIP tumors (a human prostate tumor genetically modified to overexpress hPSMA).[49] The combination human CAR T cells (injected i.v.) and a murine prostate tumor transduced to express human PSMA may not be an optimal model to explore CAR T cell therapy. However, there is the potential for interaction between anti-hPD1 Abs with mPDL-1, since PD1 shares 64% of protein identity between murine and human species, and PD-L1 shares 77% identity.[80,81] Murine PD-1 binds in vitro to both murine and human PD-L1, and human

PD-1 binds to the PD-L1 of each species. The structures of the murine PD-1 and human PD-L1 complexes[82] and that of the murine PD-1 and murine PD-L2[83] have been published. Despite the high homology and the ability for binding between different species, interspecies differences are responsible for the variation in the affinity of human and mouse PD-1 for their ligands. Since human PD-1 is relatively "flexible," it does not appear to present any significant barriers to murine ligand binding.[84]

Consistent with prior studies,[40,85] we were able to enhance CAR T cells therapy when combined with PD-1 blockade. However, the treatment response was only partial, of short-duration and sub-optimal. Other second generation CARs have been shown to be as or more effective, including the CD28- and 4-1BB-based mesothelin-targeted CAR T cells that achieved tumor eradication, but only following direct intra-pleural administration.[40]

We suggest that the limited response we observed also suggests that there are other mechanisms restricting CAR T cell trafficking and function in prostate solid tumors, which may extend to other solid tumors as well.

### Conclusions

We show that anti-hPSMA-directed CAR T cell monotherapy of subcutaneous Myc-CaP:PSMA(+) tumors is ineffective, whereas the combination of anti-hPSMA-directed CAR T cells plus anti-hPD1 mAb immune modulation provides a short-duration, sub-optimal treatment response. These results also suggest that other immune modulation mechanisms need to be brought into play to further reverse the restriction to CAR T cell targeting and persistence in hPSMA expressing Myc-CaP tumors and to provide optimal CAR T cell therapy. The results also suggest that ATP-dependent Luciferin-luciferase bioluminescence reporters should be used with caution in the monitoring of T cell trafficking and persistence, particularly when T cells transition to an activated state.

## MATERIALS AND METHODS

### Cells and Culture Conditions

The Myc-CaP androgen-dependent prostate cancer cell line, derived from a *c-myc* transgenic mouse with prostate cancer, was provided by Dr. Charles Sawyers[50] and was cultured in DMEM media supplemented with 10% FBS, 4 mM glutamine, and 5 mM glucose. Myc-CaP cancer cells were transduced with a newly generated vector SFG-hPSMA. A transgene containing human PSMA complementary DNA (cDNA) was amplified from total mRNA derived from human prostate cancer cell line LNCaP using 5′hPSMA 5′-ACATGTG GAATCTCCTTCACGAAAC-3′ and 5′-GGATCCTCGAGCTTAG GCTACTTCACTCAAAG-3′ primers set. Human PSMA cDNA was cloned into the SFG ɣ-based retroviral vector.[24,51,53] Human PSMA expression was assessed using anti-human PSMA rat antibody as described previously[24] and cells were sorted using the fluorescence-activated cell sorter (FACS) (BD Bioscience, CA, USA) several times to achieve a 100% hPSMA-positive population. Additionally, Myc-CaP:hPSMA(+) and Myc-CaP:hPSMA(−) cells were transduced with a SFG-RLuc-IRES-GFP vector[54] to detect tumor location and its relative borders. A new SFG-tdRFP/CBRluc (RFP/CBR) retroviral vector was obtained by subcloning Click Beetle Red luciferase (CBRluc) cDNA from the pCBR basic vector (Promega) into the SFG-tdRFP/Renilla luciferase (RFP/Rluc) retroviral vector by replacing the Renilla luciferase gene.[24] A new hPSMA-specific CAR retroviral vector named SFG-PIg28z was developed by inserting a CH2-CH3 domain from the human IgG heavy chain[86] in the *Not*I restriction site between the anti-hPSMA scFv and CD28 signaling motif in the SFG-P28z vector.[53] It was performed for better detectability by FACS staining with anti-human IgG antibody which is specific for the inserted region (#2040-08; Southern Biotechnology Associates).[53] For transduction we have used the PG13 producer cell lines, bearing anti-hPSMA CAR and SFG-tdRFP/CBRluc vectors. Retroviral particles were obtained using the GPG29 (H29) producer cell line and were used to infect target cells.[28] Cells were stably transduced by incubating 50% confluent cell cultures with virus-containing medium for 12 hr in presence of polybrene (8 μg/mL; Sigma-Aldrich). Cells were sorted using FACS (BD Biosciences) using GFP or tdRFP as fluorescence markers.

### Generation of Genetically Modified T Cells

SFG-PIg28z- and SFG-tdRFP/CBRluc- retroviral supernatants were produced as described above. Monocyte-depleted PBMCs were activated with anti-CD3/CD28 beads (Dynabeads; Thermo Fisher Scientific) in a 3:1 bead:cell ratio with 20 IU/mL IL-2 for 7 days. Activated T cells were then retrovirally transduced on days 3 and 4, supernatants from the different vectors were mixed on transduction days at a 1:1 ratio. Anti-CD3/CD28 beads were removed on day 7. Media and IL-2 were changed every 3 days. Transduction efficacy was confirmed by FACS after staining with anti-human IgG antibody (#2040-08; Southern Biotechnology Associates) for the detection of cells bearing anti-hPSMA vector and detection of tdRFP/CBRLuc. To assess CAR T cell function we decided to follow the clinical protocol of CAR T cell preparation.[87] Two sets of CAR T cells (from different donors) were obtained for the current study. One set of CAR T cells was utilized for the first CAR T cell trafficking experiment (Figure S2) and a Winn assay.[55] To perform anti-hPD1 mAb and anti-hPSMA CAR T cell treatment we obtained another set of CAR T cells. Transduction efficiencies varied from 87% to 99.8% for the anti-hPSMA marker after cell sorting, and between 67% and 34% for cells that were double-positive for both anti-hPSMA marker and tdRFP/CBRLuc. Cells were expanded over 18 days and cryopreserved using 2× cryopreserved medium composed of 7% Plasma-lyte, 20% of RIMSO-50 (DMSO; Mylan Institutional), 40% of albumin (human; GRIFOLS), and 33% (HESpan [hetastarch]).

T cell function studies were performed as described previously.[24] Standard $^{51}$Cr release assays were performed to evaluate CAR T cell cytolytic ability. Target tumor cells were loaded with 100 μCi of $^{51}$Cr for 1 hr, and then 10,000 tumor cells were co-incubated with CAR T cells for 6 hr at effector-to-target (E:T) ratios ranging from 40:1 to 1:1. Supernatants were harvested and $^{51}$Cr release quantified using a Gamma Counter (Packard). Percent lysis was calculated as

follows: percent lysis = (experimental lysis − spontaneous lysis)/(maximal lysis − spontaneous lysis) × 100%, where maximal lysis was induced by incubation in a 2% Triton X-100 solution.

### Metabolic Assessment of T Cells

The metabolic profiles were determined at steps of T cell stimulation and transduction to assess glycolytic function and mitochondrial respiration of T cells during stimulation, transduction and expansion. We performed a series of real-time measurements of the extracellular acidification rate (ECAR) and OCR using a Seahorse XF96 Extracellular Flux Analyzer (Agilent). The XF Analyzer (Seahorse Biosciences) simultaneously measures energy producing pathways non-invasively in real-time. For the assessment of glycolysis, cells are initially incubated without glucose and ECAR is assessed. The first injection is a saturating concentration of glucose (25 mM), where glucose is taken up by the cells and catabolized through the glycolytic pathway to lactate, producing ATP and protons. The extrusion of protons into the surrounding medium produces a rapid increase in ECAR. In the mitochondrial respiration assay, basal OCR is measured under full media growing conditions followed by sequential addition of oligomycin, FCCP, and antimycin A/rotenone with a measurement of changes in OCR. The resulting profiles show the relative contribution of non-respiratory chain oxygen consumption, ATP-linked oxygen consumption and the maximal respiration after the addition of FCCP. Data presented here represent two independent experiments at different days and were normalized to 350,000 cells.

### In Vivo Studies

NOD.SCID Il2rg$^{-/-}$ (NSG) mice were obtained from Jackson Laboratories and FVB/N male mice were from Charles River Laboratories. All mice were 5–6 weeks of age and all mice groups consisted of n = 5 per group. The animal protocol was approved by the Memorial Sloan Kettering Institutional Animal Care and Use Committee. NOD.Cg-Prkdc(scid)Il2rg were injected subcutaneously with $1 \times 10^6$ Myc-CaP:hPSMA(+) or Myc-CaP:hPSMA(−) cells in 1:1 ratio of matrigel to media in the right flank subcutaneously. Myc-CaP wild-type cells ($1 \times 10^6$) were injected into FVB/N mice. We reduced the number of CAR T cells for injection from $20 \times 10^6$ per mouse (Figure S2) to $10 \times 10^6$, in later experiments. Two independent Winn assay experiments (Figure 2) were performed. The first experiment included three mice per group, whereas the second experiment included five mice per group. The data are presented for the second and most representative experiment. For the combined treatment studies, anti-hPSMA CAR T cells were thawed and reconstituted in standard T cell media for 24 hr. Anti-hPD1 mAb or IgG-control mAb were administrated to three groups of mice 3 hours before i.v. infusion of CAR T cells, and then every other day (between days 10 and 20 of tumor growth). Three groups of mice consisted of Myc-CaP:hPSMA(+) IgG group n = 5; Myc-CaP:hPSMA(−) anti-PD1 group n = 5; and Myc-CaP:hPSMA(+) anti-PD1 groups n = 5 and n = 3. Myc-CaP:hPSMA(+) or Myc-CaP:hPSMA(−) tumors in NOD.Cg-Prkdc(scid)Il2rg mice were treated with anti-hPD-1 (human, J110) and isotype MOPC-21 (human, IgG control) antibodies. Myc-CaP wild-type tumors in FVB/N mice were treated with anti-mPD-1 (murine, clone RMP1-14), and isotype 2A3 (murine, IgG control) antibodies when tumors reached a size of ~50 mm$^3$, which occurred within ~10 days after implantation of the tumor cells. All antibodies were obtained from BioXCell. Anti-mPD1 and anti-hPD1 antibody was administered by i.p. injection, at 200 μg per mouse every other day.[88]

### Bioluminescence Imaging and Histology

BLI was performed with an IVIS SPECTRUM Imaging System (Perkin Elmer) and analyzed as described previously.[89] Tumor and lung tissue processing and staining was performed at Molecular Cytology Core Facility of Memorial Sloan Kettering Cancer Center. The stained sections were digitized and scanned using a Panoramic Viewer (3DHistech) and analyzed with MetaMorph Image Analysis Software (Molecular Devices). A fluorescence threshold was used to include only cell-specific signals and exclude background. Size and morphology filters have been applied to ensure only cells are counted (not cellular debris), and the number of immune cells were recorded. Cell sizes were obtained by applying the above thresholds and obtaining the area of each identified T cell. The data (area of individual T cels) were combined for group statistics (n = 3,621 T cells for the control group; n = 14,531 T cells for anti-PD1 group). Detailed information for CD31/PDL1, CD3$^+$, and TUNEL staining of tissues is provided in the Supplemental Material and Methods.

### Statistical Analysis

Results are presented as mean ± SD. Statistical significance was determined by a two-tailed Student's t test. $p < 0.05$ was considered significant. All data presented for T cells assessment using IFC staining were analyzed using GraphPad Prism (version 6.0; GraphPad Software) and are presented as mean ± SD. Results were analyzed using the unpaired Student's t test, and statistical significance was defined as $p < 0.05$.

## SUPPLEMENTAL INFORMATION

Supplemental Information includes Supplemental Materials and Methods and five figures and can be found with this article online at http://dx.doi.org/10.1016/j.omto.2016.11.005.

## AUTHOR CONTRIBUTIONS

Conception/design, I.S., E.M., V.P., and R.B.; Development of methodology, I.C., M. Moroz, J.Z., L.S., and I.S.; Acquisition of data, E.M., I.S., M. Mane, and M. Moroz; Analysis and interpretation of data, E.M., I.S., I.C., M. Mane, M. Moroz, V.P., and R.B.; Writing, review, and/or revision of the manuscript, I.S., I.C., V.P., and R.B.; Administrative, technical, or material support, V.P. and R.B.; Study supervision, I.S., V.P., and R.B.; Pathological diagnosis, analysis, and interpretation of the immunohistochemical data, I.S. and I.C.; and Carrying out experiments and analyzing data, E.M., I.S., M. Moroz, and I.C.

## CONFLICTS OF INTEREST

The authors declare no conflicts of interest.

## ACKNOWLEDGMENTS

We thank Nisargbai S. Shah for a technical assistance and Drs. Taha Merghoub and Susan Slovin for valuable discussions. We thank Molecular Cytology Core Facility of MSKCC, especially Drs. K. Manova-Todorova and D. Yarilin for their scientific and technical advice during staining of CAR T cells in tumors. This work was supported by the MSKCC Center for Molecular Imaging in Cancer (P50CA86438) and NIH Grants R01 CA163980, RO1 CA172846, R01 CA161138, and P30 CA008748 (MSK Cancer Center Support Grant/Core Grant).

## REFERENCES

1. Hsing, A.W., Tsao, L., and Devesa, S.S. (2000). International trends and patterns of prostate cancer incidence and mortality. Int. J. Cancer *85*, 60–67.
2. Siegel, R.L., Miller, K.D., and Jemal, A. (2015). Cancer statistics, 2015. CA Cancer J. Clin. *65*, 5–29.
3. Ning, Y.M., Gulley, J.L., Arlen, P.M., Woo, S., Steinberg, S.M., Wright, J.J., Parnes, H.L., Trepel, J.B., Lee, M.J., Kim, Y.S., et al. (2010). Phase II trial of bevacizumab, thalidomide, docetaxel, and prednisone in patients with metastatic castration-resistant prostate cancer. J. Clin. Oncol. *28*, 2070–2076.
4. Clarke, J.M., and Armstrong, A.J. (2013). Novel therapies for the treatment of advanced prostate cancer. Curr. Treat. Options Oncol. *14*, 109–126.
5. DiPaola, R.S., Plante, M., Kaufman, H., Petrylak, D.P., Israeli, R., Lattime, E., Manson, K., and Schuetz, T. (2006). A phase I trial of pox PSA vaccines (PROSTVAC-VF) with B7-1, ICAM-1, and LFA-3 co-stimulatory molecules (TRICOM) in patients with prostate cancer. J. Transl. Med. *4*, 1.
6. Kantoff, P.W., Higano, C.S., Shore, N.D., Berger, E.R., Small, E.J., Penson, D.F., Redfern, C.H., Ferrari, A.C., Dreicer, R., Sims, R.B., et al. (2010). Sipuleucel-T immunotherapy for castration-resistant prostate cancer. N. Engl. J. Med. *363*, 411–422.
7. Hillerdal, V., and Essand, M. (2015). Chimeric antigen receptor-engineered T cells for the treatment of metastatic prostate cancer. BioDrugs *29*, 75–89.
8. Sadelain, M., Rivière, I., and Brentjens, R. (2003). Targeting tumours with genetically enhanced T lymphocytes. Nat. Rev. Cancer *3*, 35–45.
9. Sadelain, M. (2009). T-cell engineering for cancer immunotherapy. Cancer J. *15*, 451–455.
10. Morello, A., Sadelain, M., and Adusumilli, P.S. (2016). Mesothelin-targeted CARs: driving T cells to solid tumors. Cancer Discov. *6*, 133–146.
11. Geiger, T.L., and Jyothi, M.D. (2001). Development and application of receptor-modified T lymphocytes for adoptive immunotherapy. Transfus. Med. Rev. *15*, 21–34.
12. Ma, Q., Gonzalo-Daganzo, R.M., and Junghans, R.P. (2002). Genetically engineered T cells as adoptive immunotherapy of cancer. Cancer Chemother. Biol. Response Modif. *20*, 315–341.
13. Altenschmidt, U., Klundt, E., and Groner, B. (1997). Adoptive transfer of in vitro-targeted, activated T lymphocytes results in total tumor regression. J. Immunol. *159*, 5509–5515.
14. Darcy, P.K., Haynes, N.M., Snook, M.B., Trapani, J.A., Cerruti, L., Jane, S.M., and Smyth, M.J. (2000). Redirected perforin-dependent lysis of colon carcinoma by ex vivo genetically engineered CTL. J. Immunol. *164*, 3705–3712.
15. Haynes, N.M., Trapani, J.A., Teng, M.W., Jackson, J.T., Cerruti, L., Jane, S.M., Kershaw, M.H., Smyth, M.J., and Darcy, P.K. (2002). Single-chain antigen recognition receptors that costimulate potent rejection of established experimental tumors. Blood *100*, 3155–3163.
16. McGuinness, R.P., Ge, Y., Patel, S.D., Kashmiri, S.V., Lee, H.S., Hand, P.H., Schlom, J., Finer, M.H., and McArthur, J.G. (1999). Anti-tumor activity of human T cells expressing the CC49-zeta chimeric immune receptor. Hum. Gene Ther. *10*, 165–173.
17. Hwu, P., Yang, J.C., Cowherd, R., Treisman, J., Shafer, G.E., Eshhar, Z., and Rosenberg, S.A. (1995). In vivo antitumor activity of T cells redirected with chimeric antibody/T-cell receptor genes. Cancer Res. *55*, 3369–3373.
18. Wang, G., Chopra, R.K., Royal, R.E., Yang, J.C., Rosenberg, S.A., and Hwu, P. (1998). A T cell-independent antitumor response in mice with bone marrow cells retrovirally transduced with an antibody/Fc-gamma chain chimeric receptor gene recognizing a human ovarian cancer antigen. Nat. Med. *4*, 168–172.
19. Chekmasova, A.A., Rao, T.D., Nikhamin, Y., Park, K.J., Levine, D.A., Spriggs, D.R., and Brentjens, R.J. (2010). Successful eradication of established peritoneal ovarian tumors in SCID-Beige mice following adoptive transfer of T cells genetically targeted to the MUC16 antigen. Clin. Cancer Res. *16*, 3594–3606.
20. Brentjens, R.J., Latouche, J.B., Santos, E., Marti, F., Gong, M.C., Lyddane, C., King, P.D., Larson, S., Weiss, M., Rivière, I., and Sadelain, M. (2003). Eradication of systemic B-cell tumors by genetically targeted human T lymphocytes co-stimulated by CD80 and interleukin-15. Nat. Med. *9*, 279–286.
21. Gade, T.P., Hassen, W., Santos, E., Gunset, G., Saudemont, A., Gong, M.C., Brentjens, R., Zhong, X.S., Stephan, M., Stefanski, J., et al. (2005). Targeted elimination of prostate cancer by genetically directed human T lymphocytes. Cancer Res. *65*, 9080–9088.
22. Adusumilli, P.S., Cherkassky, L., Villena-Vargas, J., Colovos, C., Servais, E., Plotkin, J., Jones, D.R., and Sadelain, M. (2014). Regional delivery of mesothelin-targeted CAR T cell therapy generates potent and long-lasting CD4-dependent tumor immunity. Sci. Transl. Med. *6*, 261ra151.
23. Sweat, S.D., Pacelli, A., Murphy, G.P., and Bostwick, D.G. (1998). Prostate-specific membrane antigen expression is greatest in prostate adenocarcinoma and lymph node metastases. Urology *52*, 637–640.
24. Dobrenkov, K., Olszewska, M., Likar, Y., Shenker, L., Gunset, G., Cai, S., Pillarsetty, N., Hricak, H., Sadelain, M., and Ponomarev, V. (2008). Monitoring the efficacy of adoptively transferred prostate cancer-targeted human T lymphocytes with PET and bioluminescence imaging. J Nucl Med. *49*, 1162–1170.
25. Likar, Y., Dobrenkov, K., Olszewska, M., Shenker, L., Cai, S., Hricak, H., and Ponomarev, V. (2009). PET imaging of HSV1-tk mutants with acquired specificity toward pyrimidine- and acycloguanosine-based radiotracers. Eur. J. Nucl. Med. Mol. Imaging *36*, 1273–1282.
26. Baiz, D., Hassan, S., Choi, Y.A., Flores, A., Karpova, Y., Yancey, D., Pullikuth, A., Sui, G., Sadelain, M., Debinski, W., and Kulik, G. (2013). Combination of the PI3K inhibitor ZSTK474 with a PSMA-targeted immunotoxin accelerates apoptosis and regression of prostate cancer. Neoplasia *15*, 1172–1183.
27. Gong, M.C., Chang, S.S., Sadelain, M., Bander, N.H., and Heston, W.D. (1999). Prostate-specific membrane antigen (PSMA)-specific monoclonal antibodies in the treatment of prostate and other cancers. Cancer Metastasis Rev. *18*, 483–490.
28. Gong, M.C., Latouche, J.B., Krause, A., Heston, W.D., Bander, N.H., and Sadelain, M. (1999). Cancer patient T cells genetically targeted to prostate-specific membrane antigen specifically lyse prostate cancer cells and release cytokines in response to prostate-specific membrane antigen. Neoplasia *1*, 123–127.
29. Brentjens, R.J., Davila, M.L., Riviere, I., Park, J., Wang, X., Cowell, L.G., Bartido, S., Stefanski, J., Taylor, C., Olszewska, M., et al. (2013). CD19-targeted T cells rapidly induce molecular remissions in adults with chemotherapy-refractory acute lymphoblastic leukemia. Sci. Transl. Med. *5*, 177ra38.
30. Davila, M.L., Riviere, I., Wang, X., Bartido, S., Park, J., Curran, K., Chung, S.S., Stefanski, J., Borquez-Ojeda, O., Olszewska, M., et al. (2014). Efficacy and toxicity management of 19-28z CAR T cell therapy in B cell acute lymphoblastic leukemia. Sci. Transl. Med. *6*, 224ra25.
31. Till, B.G., Jensen, M.C., Wang, J., Chen, E.Y., Wood, B.L., Greisman, H.A., Qian, X., James, S.E., Raubitschek, A., Forman, S.J., et al. (2008). Adoptive immunotherapy for indolent non-Hodgkin lymphoma and mantle cell lymphoma using genetically modified autologous CD20-specific T cells. Blood *112*, 2261–2271.
32. Pule, M.A., Savoldo, B., Myers, G.D., Rossig, C., Russell, H.V., Dotti, G., Huls, M.H., Liu, E., Gee, A.P., Mei, Z., et al. (2008). Virus-specific T cells engineered to coexpress tumor-specific receptors: persistence and antitumor activity in individuals with neuroblastoma. Nat. Med. *14*, 1264–1270.
33. Peres, E., Wood, G.W., Poulik, J., Baynes, R., Sood, S., Abidi, M.H., Klein, J., Bhambhani, K., Dansey, R., and Abella, E. (2008). High-dose chemotherapy and adoptive immunotherapy in the treatment of recurrent pediatric brain tumors. Neuropediatrics *39*, 151–156.
34. Gilham, D.E., Debets, R., Pule, M., Hawkins, R.E., and Abken, H. (2012). CAR-T cells and solid tumors: tuning T cells to challenge an inveterate foe. Trends Mol. Med. *18*, 377–384.

35. Gajewski, T.F., Woo, S.R., Zha, Y., Spaapen, R., Zheng, Y., Corrales, L., and Spranger, S. (2013). Cancer immunotherapy strategies based on overcoming barriers within the tumor microenvironment. Curr. Opin. Immunol. *25*, 268–276.

36. Fearon, D.T. (2014). The carcinoma-associated fibroblast expressing fibroblast activation protein and escape from immune surveillance. Cancer Immunol. Res. *2*, 187–193.

37. Peng, W., Ye, Y., Rabinovich, B.A., Liu, C., Lou, Y., Zhang, M., Whittington, M., Yang, Y., Overwijk, W.W., Lizée, G., and Hwu, P. (2010). Transduction of tumor-specific T cells with CXCR2 chemokine receptor improves migration to tumor and antitumor immune responses. Clin Cancer Res. *16*, 5458–5468.

38. Zhang, L., Morgan, R.A., Beane, J.D., Zheng, Z., Dudley, M.E., Kassim, S.H., Nahvi, A.V., Ngo, L.T., Sherry, R.M., Phan, G.Q., et al. (2015). Tumor-infiltrating lymphocytes genetically engineered with an inducible gene encoding interleukin-12 for the immunotherapy of metastatic melanoma. Clin Cancer Res. *21*, 2278–2288.

39. Kochenderfer, J.N., Dudley, M.E., Kassim, S.H., Somerville, R.P.T., Carpenter, R.O., Stetler-Stevenson, M., Yang, J.C., Phan, G.Q., Hughes, M.S., Sherry, R.M., et al. (2015). Chemotherapy-refractory diffuse large B-cell lymphoma and indolent B-cell malignancies can be effectively treated with autologous T cells expressing an anti-CD19 chimeric antigen receptor. J. Clin. Oncol. *33*, 540–549.

40. Cherkassky, L., Morello, A., Villena-Vargas, J., Feng, Y., Dimitrov, D.S., Jones, D.R., Sadelain, M., and Adusumilli, P.S. (2016). Human CAR T cells with cell-intrinsic PD-1 checkpoint blockade resist tumor-mediated inhibition. J. Clin. Invest. *126*, 3130–3144.

41. Stephan, S.B., Taber, A.M., Jileaeva, I., Pegues, E.P., Sentman, C.L., and Stephan, M.T. (2015). Biopolymer implants enhance the efficacy of adoptive T-cell therapy. Nat. Biotechnol. *33*, 97–101.

42. Roth, T.J., Sheinin, Y., Lohse, C.M., Kuntz, S.M., Frigola, X., Inman, B.A., Krambeck, A.E., McKenney, M.E., Karnes, R.J., Blute, M.L., et al. (2007). B7-H3 ligand expression by prostate cancer: a novel marker of prognosis and potential target for therapy. Cancer Res. *67*, 7893–7900.

43. Martin, A.M., Nirschl, T.R., Nirschl, C.J., Francica, B.J., Kochel, C.M., van Bokhoven, A., Meeker, A.K., Lucia, M.S., Anders, R.A., DeMarzo, A.M., and Drake, C.G. (2015). Paucity of PD-L1 expression in prostate cancer: innate and adaptive immune resistance. Prostate Cancer Prostatic Dis. *18*, 325–332.

44. Ebelt, K., Babaryka, G., Frankenberger, B., Stief, C.G., Eisenmenger, W., Kirchner, T., Schendel, D.J., and Noessner, E. (2009). Prostate cancer lesions are surrounded by FOXP3+, PD-1+ and B7-H1+ lymphocyte clusters. Eur. J. Cancer *45*, 1664–1672.

45. Gevensleben, H., Dietrich, D., Golletz, C., Steiner, S., Jung, M., Thiesler, T., Majores, M., Stein, J., Uhl, B., Müller, S., et al. (2015). The immune checkpoint regulator PD-L1 is highly expressed in aggressive primary prostate cancer. Clin Cancer Res. *22*, 1969–1977.

46. Momtaz, P., and Postow, M.A. (2014). Immunologic checkpoints in cancer therapy: focus on the programmed death-1 (PD-1) receptor pathway. Pharm. Genomics Pers. Med. *7*, 357–365.

47. Callahan, M.K., and Wolchok, J.D. (2013). At the bedside: CTLA-4- and PD-1-blocking antibodies in cancer immunotherapy. J. Leukoc. Biol. *94*, 41–53.

48. Zhong, X.S., Matsushita, M., Plotkin, J., Riviere, I., and Sadelain, M. (2010). Chimeric antigen receptors combining 4-1BB and CD28 signaling domains augment PI3kinase/AKT/Bcl-XL activation and CD8+ T cell-mediated tumor eradication. Mol. Ther. *18*, 413–420.

49. Zuccolotto, G., Fracasso, G., Merlo, A., Montagner, I.M., Rondina, M., Bobisse, S., Figini, M., Cingarlini, S., Colombatti, M., Zanovello, P., and Rosato, A. (2014). PSMA-specific CAR-engineered T cells eradicate disseminated prostate cancer in preclinical models. PLoS ONE *9*, e109427.

50. Watson, P.A., Ellwood-Yen, K., King, J.C., Wongvipat, J., Lebeau, M.M., and Sawyers, C.L. (2005). Context-dependent hormone-refractory progression revealed through characterization of a novel murine prostate cancer cell line. Cancer Res. *65*, 11565–11571.

51. Rivière, I., Brose, K., and Mulligan, R.C. (1995). Effects of retroviral vector design on expression of human adenosine deaminase in murine bone marrow transplant recipients engrafted with genetically modified cells. Proc. Natl. Acad. Sci. USA *92*, 6733–6737.

52. Ponomarev, V., Doubrovin, M., Serganova, I., Beresten, T., Vider, J., Shavrin, A., Ageyeva, L., Balatoni, J., Blasberg, R., and Tjuvajev, J.G. (2003). Cytoplasmically retargeted HSV1-tk/GFP reporter gene mutants for optimization of noninvasive molecular-genetic imaging. Neoplasia *5*, 245–254.

53. Maher, J., Brentjens, R.J., Gunset, G., Rivière, I., and Sadelain, M. (2002). Human T-lymphocyte cytotoxicity and proliferation directed by a single chimeric TCRzeta /CD28 receptor. Nat. Biotechnol. *20*, 70–75.

54. Huang, R., Vider, J., Serganova, I., and Blasberg, R.G. (2011). ATP-binding cassette transporters modulate both coelenterazine- and D-luciferin-based bioluminescence imaging. Mol. Imaging *10*, 215–226.

55. Genovesi, E.V., Pettey, C.L., and Collins, J.J. (1984). Use of adoptive transfer and Winn assay procedures in the further analysis of antiviral acquired immunity in mice protected against Friend leukemia virus-induced disease by passive serum therapy. Cancer Res. *44*, 1489–1498.

56. Morán, M., Rivera, H., Sánchez-Aragó, M., Blázquez, A., Merinero, B., Ugalde, C., Arenas, J., Cuezva, J.M., and Martín, M.A. (2010). Mitochondrial bioenergetics and dynamics interplay in complex I-deficient fibroblasts. Biochim. Biophys. Acta *1802*, 443–453.

57. Grupp, S.A., Kalos, M., Barrett, D., Aplenc, R., Porter, D.L., Rheingold, S.R., Teachey, D.T., Chew, A., Hauck, B., Wright, J.F., et al. (2013). Chimeric antigen receptor-modified T cells for acute lymphoid leukemia. N. Engl. J. Med. *368*, 1509–1518.

58. Kochenderfer, J.N., and Rosenberg, S.A. (2013). Treating B-cell cancer with T cells expressing anti-CD19 chimeric antigen receptors. Nat. Rev. Clin. Oncol. *10*, 267–276.

59. Tsushima, F., Yao, S., Shin, T., Flies, A., Flies, S., Xu, H., Tamada, K., Pardoll, D.M., and Chen, L. (2007). Interaction between B7-H1 and PD-1 determines initiation and reversal of T-cell anergy. Blood *110*, 180–185.

60. Taube, J.M., Klein, A., Brahmer, J.R., Xu, H., Pan, X., Kim, J.H., Chen, L., Pardoll, D.M., Topalian, S.L., and Anders, R.A. (2014). Association of PD-1, PD-1 ligands, and other features of the tumor immune microenvironment with response to anti-PD-1 therapy. Clin. Cancer Res. *20*, 5064–5074.

61. Topalian, S.L., Hodi, F.S., Brahmer, J.R., Gettinger, S.N., Smith, D.C., McDermott, D.F., Powderly, J.D., Carvajal, R.D., Sosman, J.A., Atkins, M.B., et al. (2012). Safety, activity, and immune correlates of anti-PD-1 antibody in cancer. N. Engl. J. Med. *366*, 2443–2454.

62. Jiang, Y., Li, Y., and Zhu, B. (2015). T-cell exhaustion in the tumor microenvironment. Cell Death Dis. *6*, e1792.

63. Tumeh, P.C., Harview, C.L., Yearley, J.H., Shintaku, I.P., Taylor, E.J., Robert, L., Chmielowski, B., Spasic, M., Henry, G., Ciobanu, V., et al. (2014). PD-1 blockade induces responses by inhibiting adaptive immune resistance. Nature *515*, 568–571.

64. June, C.H., Ledbetter, J.A., Gillespie, M.M., Lindsten, T., and Thompson, C.B. (1987). T-cell proliferation involving the CD28 pathway is associated with cyclosporine-resistant interleukin 2 gene expression. Mol. Cell. Biol. *7*, 4472–4481.

65. Teague, T.K., Munn, L., Zygourakis, K., and McIntyre, B.W. (1993). Analysis of lymphocyte activation and proliferation by video microscopy and digital imaging. Cytometry *14*, 772–782.

66. Moon, E.K., Ranganathan, R., Eruslanov, E., Kim, S., Newick, K., O'Brien, S., Lo, A., Liu, X., Zhao, Y., and Albelda, S.M. (2016). Blockade of Programmed Death 1 Augments the Ability of Human T Cells Engineered to Target NY-ESO-1 to Control Tumor Growth after Adoptive Transfer. Clin. Cancer Res. *22*, 436–447.

67. Shi, H., Sun, M., Liu, L., and Wang, Z. (2014). Chimeric antigen receptor for adoptive immunotherapy of cancer: latest research and future prospects. Mol. Cancer *13*, 219.

68. Brentjens, R.J., Rivière, I., Park, J.H., Davila, M.L., Wang, X., Stefanski, J., Taylor, C., Yeh, R., Bartido, S., Borquez-Ojeda, O., et al. (2011). Safety and persistence of adoptively transferred autologous CD19-targeted T cells in patients with relapsed or chemotherapy refractory B-cell leukemias. Blood *118*, 4817–4828.

69. Porter, D.L., Hwang, W.T., Frey, N.V., Lacey, S.F., Shaw, P.A., Loren, A.W., Bagg, A., Marcucci, K.T., Shen, A., Gonzalez, V., et al. (2015). Chimeric antigen receptor T cells persist and induce sustained remissions in relapsed refractory chronic lymphocytic leukemia. Sci. Transl. Med. *7*, 303ra139.

70. Maude, S.L., Teachey, D.T., Porter, D.L., and Grupp, S.A. (2015). CD19-targeted chimeric antigen receptor T-cell therapy for acute lymphoblastic leukemia. Blood *125*, 4017–4023.

71. Anurathapan, U., Chan, R.C., Hindi, H.F., Mucharla, R., Bajgain, P., Hayes, B.C., Fisher, W.E., Heslop, H.E., Rooney, C.M., Brenner, M.K., et al. (2014). Kinetics of tumor destruction by chimeric antigen receptor-modified T cells. Mol. Ther. *22*, 623–633.

72. Robbins, P.F., Dudley, M.E., Wunderlich, J., El-Gamil, M., Li, Y.F., Zhou, J., Huang, J., Powell, D.J., Jr., and Rosenberg, S.A. (2004). Cutting edge: persistence of transferred lymphocyte clonotypes correlates with cancer regression in patients receiving cell transfer therapy. J. Immunol. *173*, 7125–7130.

73. Kakarla, S., and Gottschalk, S. (2014). CAR T cells for solid tumors: armed and ready to go? Cancer J. *20*, 151–155.

74. Fox, C.J., Hammerman, P.S., and Thompson, C.B. (2005). Fuel feeds function: energy metabolism and the T-cell response. Nat. Rev. Immunol. *5*, 844–852.

75. Frauwirth, K.A., and Thompson, C.B. (2004). Regulation of T lymphocyte metabolism. J. Immunol. *172*, 4661–4665.

76. Scharping, N.E., Menk, A.V., Moreci, R.S., Whetstone, R.D., Dadey, R.E., Watkins, S.C., Ferris, R.L., and Delgoffe, G.M. (2016). The tumor microenvironment represses T cell mitochondrial biogenesis to drive intratumoral T cell metabolic insufficiency and dysfunction. Immunity *45*, 374–388.

77. Thorne, N., Inglese, J., and Auld, D.S. (2010). Illuminating insights into firefly luciferase and other bioluminescent reporters used in chemical biology. Chem. Biol. *17*, 646–657.

78. Cao, Y.A., Bachmann, M.H., Beilhack, A., Yang, Y., Tanaka, M., Swijnenburg, R.J., Reeves, R., Taylor-Edwards, C., Schulz, S., Doyle, T.C., et al. (2005). Molecular imaging using labeled donor tissues reveals patterns of engraftment, rejection, and survival in transplantation. Transplantation *80*, 134–139.

79. Santos, E.B., Yeh, R., Lee, J., Nikhamin, Y., Punzalan, B., Punzalan, B., La Perle, K., Larson, S.M., Sadelain, M., and Brentjens, R.J. (2009). Sensitive in vivo imaging of T cells using a membrane-bound Gaussia princeps luciferase. Nat. Med. *15*, 338–344.

80. Freeman, G.J., Long, A.J., Iwai, Y., Bourque, K., Chernova, T., Nishimura, H., Fitz, L.J., Malenkovich, N., Okazaki, T., Byrne, M.C., et al. (2000). Engagement of the PD-1 immunoinhibitory receptor by a novel B7 family member leads to negative regulation of lymphocyte activation. J. Exp. Med. *192*, 1027–1034.

81. Zhang, X., Schwartz, J.C.D., Guo, X., Bhatia, S., Cao, E., Lorenz, M., Cammer, M., Chen, L., Zhang, Z.Y., Edidin, M.A., et al. (2004). Structural and functional analysis of the costimulatory receptor programmed death-1. Immunity *20*, 337–347.

82. Lin, D.Y., Tanaka, Y., Iwasaki, M., Gittis, A.G., Su, H.P., Mikami, B., Okazaki, T., Honjo, T., Minato, N., and Garboczi, D.N. (2008). The PD-1/PD-L1 complex resembles the antigen-binding Fv domains of antibodies and T cell receptors. Proc. Natl. Acad. Sci. USA *105*, 3011–3016.

83. Lázár-Molnár, E., Yan, Q., Cao, E., Ramagopal, U., Nathenson, S.G., and Almo, S.C. (2008). Crystal structure of the complex between programmed death-1 (PD-1) and its ligand PD-L2. Proc. Natl. Acad. Sci. USA *105*, 10483–10488.

84. Cheng, X., Veverka, V., Radhakrishnan, A., Waters, L.C., Muskett, F.W., Morgan, S.H., Huo, J., Yu, C., Evans, E.J., Leslie, A.J., et al. (2013). Structure and interactions of the human programmed cell death 1 receptor. J. Biol. Chem. *288*, 11771–11785.

85. John, L.B., Devaud, C., Duong, C.P., Yong, C.S., Beavis, P.A., Haynes, N.M., Chow, M.T., Smyth, M.J., Kershaw, M.H., and Darcy, P.K. (2013). Anti-PD-1 antibody therapy potently enhances the eradication of established tumors by gene-modified T cells. Clin Cancer Res. *19*, 5636–5646.

86. Hombach, A., Schneider, C., Sent, D., Koch, D., Willemsen, R.A., Diehl, V., Kruis, W., Bolhuis, R.L., Pohl, C., and Abken, H. (2000). An entirely humanized CD3 zeta-chain signaling receptor that directs peripheral blood t cells to specific lysis of carcinoembryonic antigen-positive tumor cells. Int. J. Cancer *88*, 115–120.

87. Wang, X., and Rivière, I. (2015). Manufacture of tumor- and virus-specific T lymphocytes for adoptive cell therapies. Cancer Gene Ther. *22*, 85–94.

88. Serganova, I., Rizwan, A., Ni, X., Thakur, S.B., Vider, J., Russell, J., Blasberg, R., and Koutcher, J.A. (2011). Metabolic imaging: a link between lactate dehydrogenase A, lactate, and tumor phenotype. Clin. Cancer Res. *17*, 6250–6261.

89. Moroz, E., Carlin, S., Dyomina, K., Burke, S., Thaler, H.T., Blasberg, R., and Serganova, I. (2009). Real-time imaging of HIF-1alpha stabilization and degradation. PLoS ONE *4*, e5077.